Bioresources and Bioprocessing

RESEARCH

Open Access

Enhancement of acetate production in hydrogen-mediated microbial electrosynthesis reactors by addition of silica nanoparticles

Zeyan Pan[1], Zhuangzhuang Liu[1,2], Xiaona Hu[3], Kai Cui[1], Wenfang Cai[1] and Kun Guo[1*]

Abstract

Microbial electrosynthesis (MES) is a promising technology for CO_2 fixation and electrical energy storage. Currently, the low current density of MES limits its practical application. The H_2-mediated and non-biofilm-driven MES could work under higher current density, but it is difficult to achieve high coulombic efficiency (CE) due to low H_2 solubility and poor mass transfer. Here, we proposed to enhance the hydrogen mass transfer by adding silica nanoparticles to the reactor. At pH 7, 35 ℃ and 39 $A{\cdot}m^{-2}$ current density, with the addition of 0.3wt% silica nanoparticles, the volumetric mass transfer coefficient (k_{La}) of H_2 in the reactor increased by 32.4% (from 0.37 h^{-1} to 0.49 h^{-1}), thereby increasing the acetate production rate and CE of the reactor by 69.8% and 69.2%, respectively. The titer of acetate in the reactor with silica nanoparticles (18.5 $g{\cdot}L^{-1}$) was 56.9% higher than that of the reactor without silica nanoparticles (11.8 $g{\cdot}L^{-1}$). Moreover, the average acetate production rate of the reactor with silica nanoparticles was up to 2.14 $g{\cdot}L^{-1}{\cdot}d^{-1}$ in the stable increment phase, which was much higher than the other reported reactors. These results demonstrated that the addition of silica nanoparticles is an effective approach to enhancing the performance of H_2-mediated MES reactors.

Keywords Microbial electrosynthesis, H_2-mediated, Silica nanoparticles, Mass transfer, Acetate production

*Correspondence:
Kun Guo
kun.guo@xjtu.edu.cn
Full list of author information is available at the end of the article

Graphical Abstract

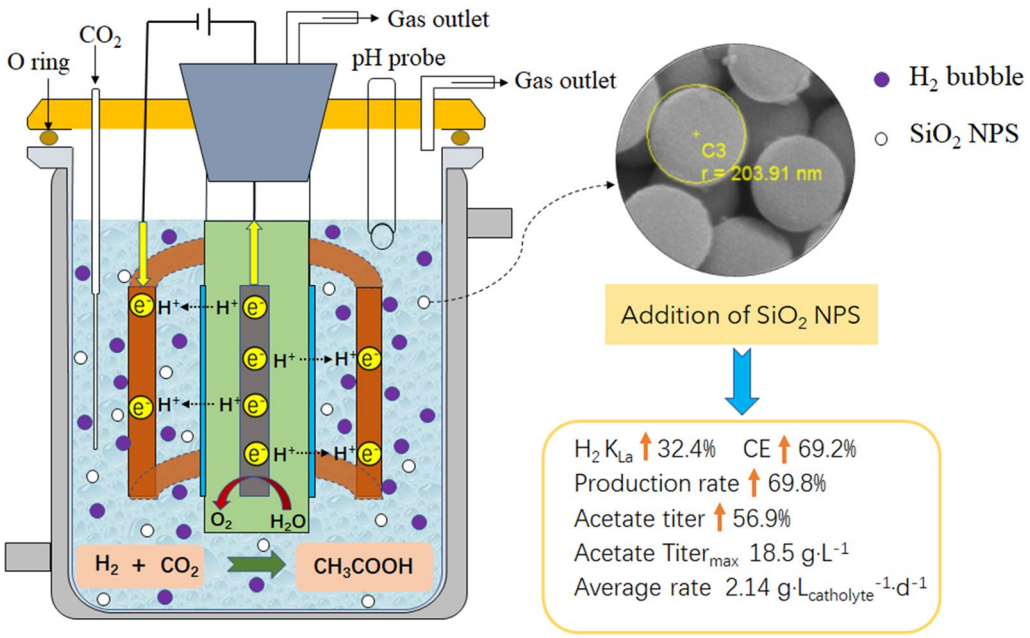

Introduction

Microbial electrosynthesis (MES) is a process that utilizes microorganisms as the cathodic catalysts for electrochemical CO_2 reduction (Nevin et al. 2011). Compared to abiotic catalysts, microorganisms have the advantages of high selectivity, self-regenerating ability, and capability of producing multi-carbon organics (Salehizadeh et al. 2020). Consequently, MES has drawn increasing attention in the fields of CO_2 valorization and renewable energy stargate (Logan & Rabaey 2012). The concept of MES emerged around 2010 after some methanogens (Cheng & Logan 2007) and acetogens were found to be able to uptake electrons from the cathode for the production of methane and acetate, respectively. After that, a lot of work has been done to modify electrode materials, discover effective microorganisms, understand extracellular electron transfer (EET) mechanisms, and develop novel reactor configurations (Aryal et al. 2017; Krieg et al. 2014). The current density (i.e., productivity) of MES has improved a lot, but it is too low to bring this technology onto the market (Jourdin & Burdyny 2021; Prevoteau et al. 2020).

Figure 1 shows the working principle of MES. In this system, renewable electricity is used to oxidize H_2O to form O_2, H^+, and e^- in the anodic chamber, and then H^+ and e^- are transported to the cathode chamber in which they are used by autotrophic microbes to fix CO_2 for organic matter production. The conventional MES was driven by the biofilm on the cathode surface, because biofilm enabled high coulombic efficiency (CE), low energy input, and good biomass retention (Fruehauf et al. 2020). However, the current density of the biofilm-driven MES was limited by the activity of the biomass and the mass transfer efficiency. Currently, the current density of cathodic biofilms has reached the maximum values of electro-active biofilms (i.e., 10–100 $A{\cdot}m^{-2}$) (Claassens et al. 2019). Thus, it is very challenging to further increase the current density of biofilm-driven MES, especially for its large-scale applications. Therefore, non-biofilm-driven MES has been proposed recently. This non-biofilm-driven MES used suspended biomass and

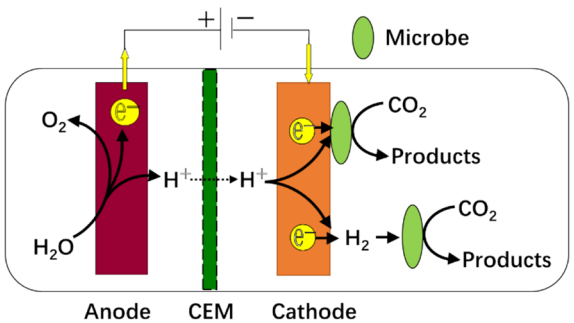

Fig. 1 The schematic of MES reactors (CEM: cation exchange membrane)

hydrogen produced from the cathode for CO_2 conversion, which was also named H_2-mediated MES. Without the limitation of biofilm, high current density could be applied to the reactor for hydrogen production. However, the low solubility and poor mass transfer of H_2 make it difficult to achieve high CE under high current density for this type of H_2-mediated MES (Liu et al. 2016).

Previously, it has been reported that the enhancement of H_2 mass transfer is an effective method to improve the performance of H_2-mediated MES reactors. For example, Rodrigues et al. reported that adding perfluorocarbon nanoemulsion (a hydrogen carrier) into H_2-mediated MES increased the productivity of acetate by 190% and obtained a CE of nearly 100% (Rodrigues et al. 2019). Our group also found that adding porous polyurethane (PPU) particles could promote the hydrogen uptake efficiency and acetate production rate in an H_2-mediated MES reactor (Xue et al. 2022). Moreover, nanoparticles have also been applied to syngas fermentation and methane fermentation to improve the gas–liquid mass transfer (Kim et al. 2014; Zhu et al. 2008). Therefore, we hypothesized that introducing nanoparticles to H_2-mediated MES may also enhance the hydrogen mass transfer, CE and acetate production rate. Among all reported nanoparticles, silica nanoparticles (SiO_2 NPS) are biocompatible, dispersible in water, and commercially available at a relatively cheap price. Compared to perfluorocarbon nanoemulsion, SiO_2 NPS can be easily separated from the fermentation broth for reuse. The PPU particles are on a millimeter scale, so that they can be easily maintained in the reactor, but the specific surface area of PPU is rather limited when compared to SiO_2 NPS. Adding SiO_2 NPS may further improve the hydrogen mass transfer in H_2-mediated reactors. Thus, the goal of this study was to investigate whether the addition of SiO_2 NPS could enhance the hydrogen mass transfer and the performance of an H_2-mediated MES.

Our experimental results showed that the addition of SiO_2 NPS in the MES system could significantly increase the H_2 mass transfer rate and H_2 solubility in water, thereby increasing the acetate production rate by 69.8% and the acetate titer by 56.9%. The average acetate production rate of the reactor with silica nanoparticles (2.14 $g{\cdot}L^{-1}{\cdot}d^{-1}$) was higher than those of the reported MES reactors. These results demonstrated adding SiO_2 NPS is an efficient way to enhance the performance of H_2-mediated MES reactors. The method reported here dramatically increases the current density and coulombic efficiency of H_2-mediated MES reactors. It can not only be applied in H_2-mediated MES reactors for acetate and methane production but also in other H_2-dependent reactions, such as biologically catalyzed N_2 fixation, CH_4 functionalization and microbial protein production.

Materials and methods

Reactor design and construction

An electrochemical continuous stirred-tank reactor (E-CSTR) was used for this study. The design of the E-CSTR is shown in Fig. 2. The reactor consisted of a tubular anode membrane assembly and a jacketed mixing vessel (outer diameter: 12.4 cm, inner diameter: 10.7 cm, height: 14.5 cm, maximum volume: 1 L). The anode membrane assembly consisted of a lid and a tubular membrane cell (diameter: 3.5 cm, height: 12.5 cm) that was placed in the middle of the lid. The bottom of the anode chamber was sealed by a PVC cap, while the top was plugged with a rubber stopper. The rubber stopper held the anode and an anode gas outlet tube. The size of the cation exchange membrane (CMI-7000, Membranes International Inc., USA) window on the anode membrane assembly was 42 cm^2 (6 cm × 7 cm). There were six openings on the lid of the reactor, and they were used for the Stainless steel bar cathode current collector, CO_2 inlet tube, base dosing tube, pH probe, cathode gas outlet tube, and liquid sample port. A stainless-steel mesh cylinder (length: 16 cm, height: 8 cm, thickness: 0.3 mm, Anguo Chengli Metal Co., Ltd., China) was used as the cathode. An IrO_2-coated titanium mesh plate (width: 3.2 cm, height: 8 cm, Baoji Zhiming Special Metal Co., Ltd., China) was used as the anode. The reactor lid and the flange of the mixing vessel were sealed by an O-ring and a clamp.

The working volume of the anolyte and catholyte was 100 mL and 600 mL, respectively. The anolyte was 0.2 $mol{\cdot}L^{-1}$ Na_2SO_4 solution, and its pH was adjusted to 2 with H_2SO_4. The catholyte was a modified M9 medium containing 6 $g{\cdot}L^{-1}$ Na_2HPO_4, 3 $g{\cdot}L^{-1}$ KH_2PO_4, 0.5 $g{\cdot}L^{-1}$ NH_4Cl, 0.5 $g{\cdot}L^{-1}$ NaCl, 0.1 $g{\cdot}L^{-1}$ $MgSO_4{\cdot}7H_2O$, 0.0146 $g{\cdot}L^{-1}$ $CaCl_2$, 4 $g{\cdot}L^{-1}$ $NaHCO_3$, 1 $ml{\cdot}L^{-1}$ trace element solution and 1 $ml{\cdot}L^{-1}$ vitamin solution. The compositions of the trace element solution and vitamin solution were provided in Table S1. The jacketed mixing vessel was connected to a recirculating water bath (DC-1006, Ningbo Scientz Biotechnology Co., Ltd., China) to control the reactor temperature. A magnetic stirrer was placed at the bottom of the vessel to control the agitation intensity of the catholyte. The anode and cathode were connected to the positive and negative terminals of the DC power supply (KA3005P, Korad Technology Co., Ltd., China), respectively. The pH of the catholyte was controlled with a pH controller (pH3.0-NI2-AC, Huzhou Tianze Biotechnology Co., Ltd., China) by automatically dosing 5 M NaOH. The reactor was equipped with a mass flow controller (D07-7, Beijing Sevenstar Flow Co., Ltd, China) to control the CO_2 flow rate. A water displacement column (filled with 1200 mL 1 mM HCl) was

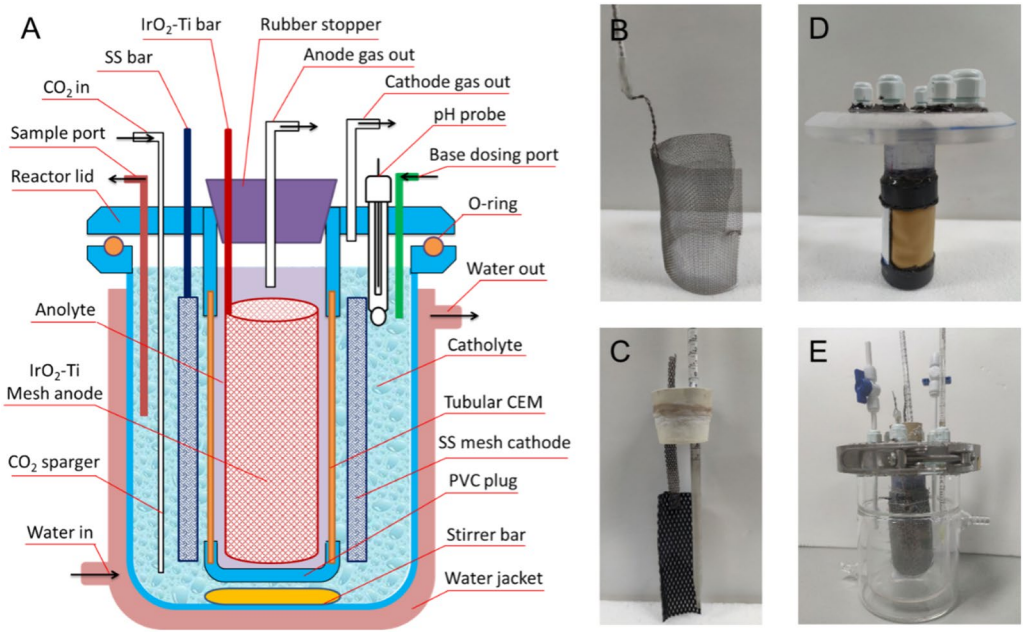

Fig. 2 The schematic of the E-CSTR reactor (**A**) and photos of the reactor parts (**B**: the cathode; **C**: the anode; **D**: the anode membrane assembly; **E**: the jacketed mixing vessel)

connected to the reactor to collect the offgas for gas flow rate and composition measurement.

Reactor startup and operational procedure

Two reactors were run in parallel, one as the control and the other one as the experimental reactor. The SiO_2 NPS used in this study were commercial hydrophilic SiO_2 NPS that was produced by the sol–gel method (average diameter 200 nm, Hebei Juli Metal Material Co., Ltd., China). The SiO_2 NPS could easily disperse in water so they were used as purchased without any pretreatment.

In the control reactor, no SiO_2 NPS were added, while in the experimental reactor 0.3wt% SiO_2 NPS were added (1.8 g of SiO_2 NPS were added into 600 mL of catholyte). The dosage of the SiO_2 NPS (0.3wt%) was chosen based on literature regarding syngas fermentation enhancement by adding SiO_2 NPS (Kim et al. 2014).

The reactor temperature was controlled at 35 ± 0.5 ℃ by the water bath, and the stirring rate of the magnetic stirrer was set at 650 rpm. The catholyte of the reactor was first flushed with N_2 for 30 min to remove the dissolved oxygen. Then, the cathode chamber was inoculated with an enriched acetate-producing mixed culture that was dominated by *Acetobacterium*. The reactor was operated in a galvanostatic mode with a starting current of 0.25 A and then switched to 0.5 A. At 0.25 and 0.5A, the CO_2 flow rate was controlled at 1.96 and 3.92 mL·min^{-1}, respectively, which resulted in an H_2/CO_2 molar ratio of 2:1. The pH of the catholyte was controlled at 7 using the pH controller.

Each day, 2 mL of catholyte was taken to measure the pH and VFAs, and the same amount of fresh catholyte was added. Occasionally, fresh anolyte was added to the anode chamber to compensate for the water loss. The reactors were operated in fed-batch mode. When the acetate concentration stopped increasing, 90% of the catholyte was replaced with a fresh medium to start a new batch. In the second batch, 0.3wt% SiO_2 NPS were added to the experimental reactor.

Analytical methods

Gas analysis

Gas samples were taken from the water displacement column to analyze the volume and composition of the unused gas. The gas composition, i.e., the concentrations of H_2 and CO_2, was analyzed by a compact gas chromatograph (GC, 7890B, Agilent). Details of the method could be found in our previous publication (Cai et al. 2022).

VFAs analysis

Liquid samples were taken from the reactor to analyze the concentration of acetate. The liquid samples were first extracted by diethyl ether and then injected into gas chromatography (GC-2010 Pro, AOC-201, Shimadzu, Japan) with an FID detector to analyze. Details of these

methods could be found in our previous publication (Cai et al. 2022).

Hydrogen mass transfer coefficient measurement

The volumetric mass transfer coefficient (K_{La}, h^{-1}) which describes the transfer resistance at the gas–liquid interface was tested by the dynamic-gasing method described in a previous article (Beckers et al. 2015). Briefly, the reactor was filled with M9 medium without inoculum. The temperature was kept at 35 ℃. The reactor was equipped with a dissolved hydrogen sensor (Clean, DH200, China) at the cover to measure and record dissolved H_2 concentrations. The K_{La} of H_2 in the reactor with SiO_2 NPS and that without SiO_2 NPS were measured under 0.5 A in abiotic conditions. For each experiment, the reactor was degassed with N_2 to remove H_2 before electrolysis. The values of the dissolved hydrogen sensor were recorded once a minute until reaching saturation.

Calculations

The k_{La} was calculated according to the adsorbing equation (Myung et al. 2016):

$$\frac{dC}{dt} = K_L a\left(C^* - C\right) \tag{1}$$

Here, C^* is the saturated concentration of dissolved hydrogen (mg H_2 L^{-1}), K_L is the mass transfer coefficient ($cm \cdot h^{-1}$), and a is the gas/liquid interfacial area per volume of liquid ($cm^2 \cdot cm^{-3}$).

The CE was calculated as described earlier (Liu et al. 2015), to reflect the productivity of the system:

$$CE = \frac{\Delta C_{HAc}(\text{mol L}^{-1}) \times V_{solution}(\text{L}) \times 8 \times F\ (\text{C mol}^{-1})}{\text{Overall charge (C)}} \times 100\% \tag{2}$$

Here, ΔC_{HAc} ($mol \cdot L^{-1}$) is the change in the concentration of acetate during the experiment, $V_{solution}$ is the total volume of the solution in the cathode chamber, and 'Overall charge' is the total electric charge passing through the cathode chamber and F is the Faraday's constant.

Results and discussion

k_{La} determination and dissolved H_2 concentration

The K_{La} was measured under different conditions to determine the mass transfer rate of dissolved H_2 at the gas–liquid interface (Fig. 3B). At 0.5 A, the K_{La} of the reactor added with SiO_2 NPS reached 0.49 h^{-1}, which was 32.4% higher than that reached without SiO_2 NPS (0.37 h^{-1}). The relation between the dissolved H_2 concentration and the electrolysis time is shown in Fig. 3A. With the addition of SiO_2 NPS, the saturated dissolved H_2 concentration increased from 1.04 $mg \cdot L^{-1}$ to 1.11 $mg \cdot L^{-1}$ at 0.5 A. All these results confirmed that adding SiO_2 NPS to the catholyte could improve the mass transfer of the dissolved H_2 in the gas–liquid interface and increase the saturated dissolved H_2 concentration of the reactor.

The kinetics of H_2 oxidation by hydrogenase is rate-dependent for H_2-induced CO_2 reduction. As H_2 has a limited solubility of 0.79 mM (Liu et al. 2016) in water at ambient conditions. Based on the information obtained from our experiments, the H_2 K_{La} of the reactors could be increased by introducing SiO_2 NPS. The improvement of the mass transfer coefficient by the interaction between nanoparticles and the gas–liquid interface could be

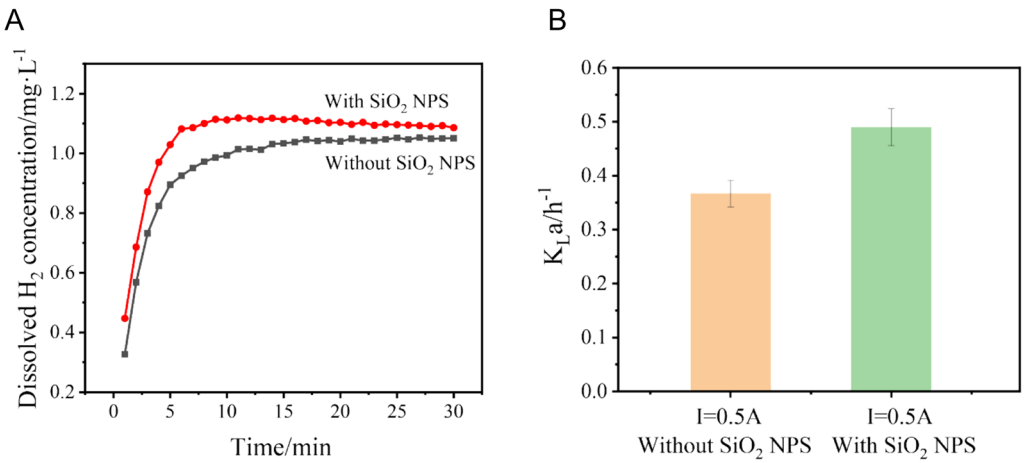

Fig. 3 The dissolved H_2 concentration curves (**A**) and the K_{La} of H_2 (**B**) of reactors at 0.5 A under abiotic conditions

explained by three theories: a shuttling or grazing effect, hydrodynamic influences at the gas–liquid interface, and changes in the specific gas–liquid interfacial area (Kim et al. 2014). The diameter of the nanoparticles was much smaller than that of the gas–liquid boundary layer, which is usually 5–25 μm. Therefore, it was likely that shuttling or grazing effects played an important role in improving gas–liquid mass transfer (Kim et al. 2014).

Acetate production

As shown in Fig. 4B, the acetate production rate was lower than 0.50 $g{\cdot}L^{-1}{\cdot}d^{-1}$ in the first 2 days, but it increased sharply in the coming days. When SiO_2 NPS were present in the reactor, the acetate concentration increased from 0.29 $g{\cdot}L^{-1}$ to 13.1 $g{\cdot}L^{-1}$ (2–8 days), and the average acetate production rate reached 2.14 $g{\cdot}L^{-1}{\cdot}d^{-1}$ in batch 1. In contrast, the acetate production rate and the final acetate concentration of the experiment without SiO_2 NPS were only 1.16 $g{\cdot}L^{-1}{\cdot}d^{-1}$ and 7.22 $g{\cdot}L^{-1}$ in batch 1, respectively. The second batch displayed a comparable production profile, but the acetate titer outperformed the first batch. The maximum acetate concentration and average acetate production rate (10–18 days) of the experiments in batch 2 with (without) particles were 18.5 (11.8) $g{\cdot}L^{-1}$ and 2.14 (1.26) $g{\cdot}L^{-1}{\cdot}d^{-1}$, respectively.

The performance of the second batch was superior to the first batch in terms of acetate titer due to the enrichment of more acetate-tolerating microorganisms during the long-term operation. In batch 2, the acetate production rate with nanoparticles was 1.7 times higher than that without nanoparticles at the stable increment stage (10–18 days) of acetate, and the titer of acetate increased by 56.9%. All these results suggested that the addition of SiO_2 NPS could improve both the acetate production rate and titer of acetate by enhancing the mass transfer of the dissolved H_2 at the gas–liquid interface and increasing the saturated dissolved H_2 concentration in the reactor. This could be attributed to the fact that enhanced gas–liquid mass transfer would normally increase the amount of biomass in the reactor (Xue et al. 2022).

Electron balance

Based on the VFAs concentration and the H_2 left in the reactor, the electron balance was calculated. Most of the electrons from the cathode ended up in acetate and H_2, while the rest could be attributed to other VFAs and biomass (Fig. 5). In general, the percentage of electrons that went to acetate increased at first and then decreased over time, whereas the percentage of electrons that ended in H_2 decreased at first and then increased over time. In batch 1, the average percentages of electrons that went to the acetate of the reactor with and without SiO_2 NPS were 36% and 19%, respectively. In the stable increment phase (10–18 days) of batch 2, the average percentage of electrons went to acetate, other VFAs and biomass, and H_2 were 44%, 41%, and 15% with SiO_2 NPS, while those without SiO_2 NPS were 26%, 28%, and 46%, respectively. Therefore, the addition of SiO_2 NPS could make more electrons go to acetate instead of H_2.

In the stable increment phase, the reactor without SiO_2 NPS reached its throughput bottleneck, because 50% of the electrical H_2 was not utilized by the culture due to the limitation of H_2 solubility in water. In contrast, the addition of SiO_2 NPS can alleviate the throughput bottleneck

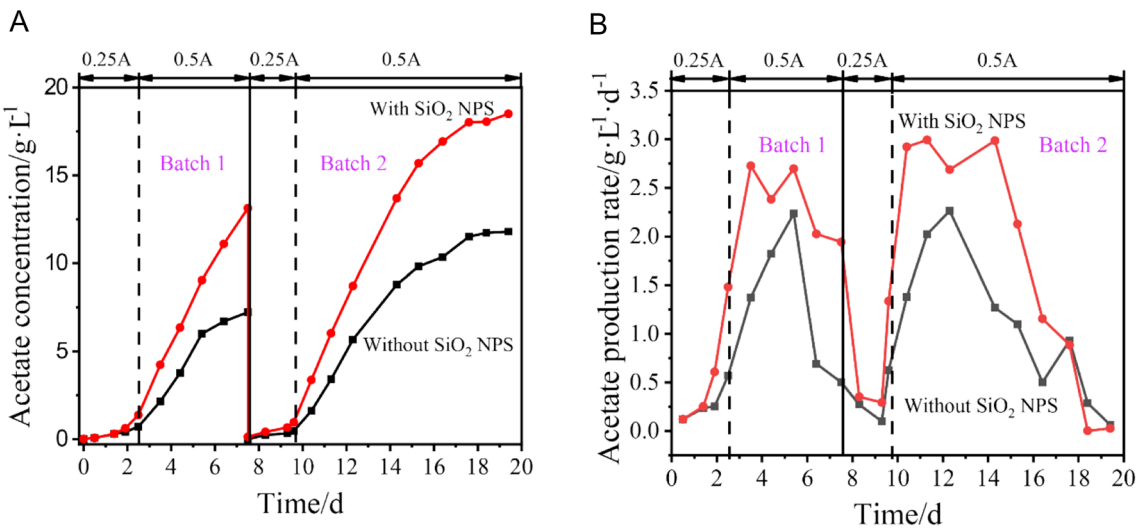

Fig. 4 The acetate concentration (**A**) and acetate production rate (**B**) of the MES reactor in two batches

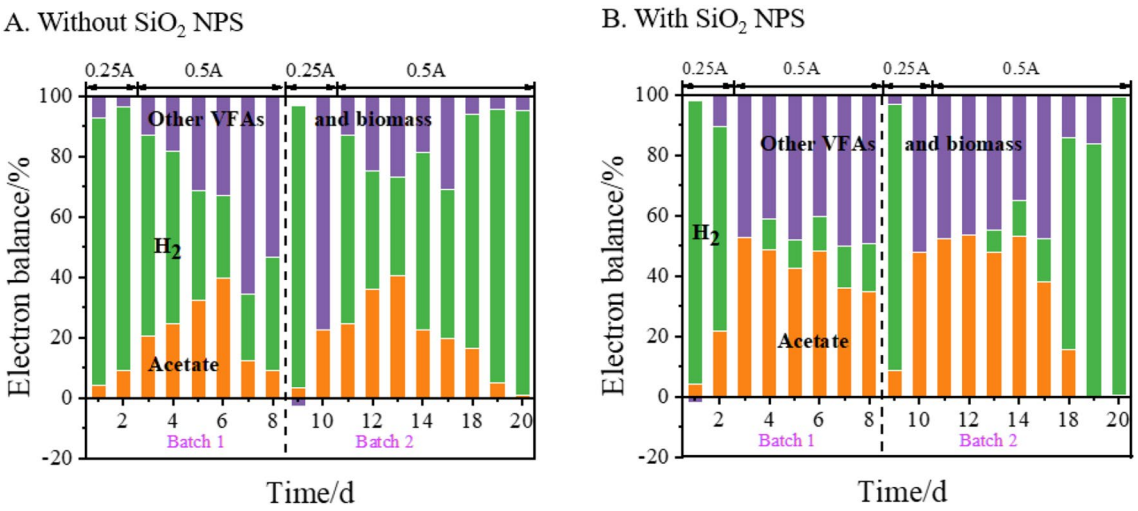

Fig. 5 The electron balance of the MES reactor in two batches

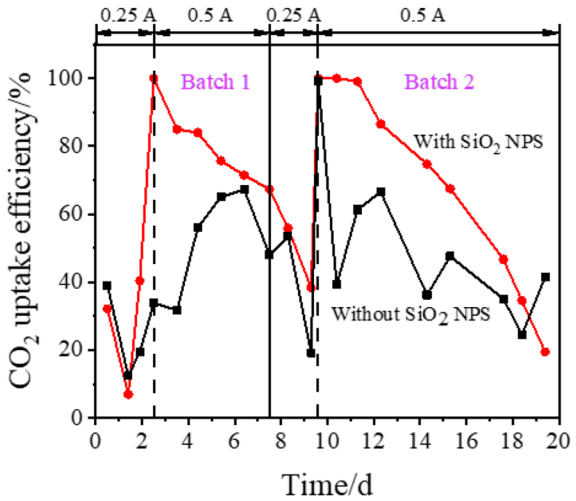

Fig. 6 CO_2 uptake efficiency of the MES reactor in two batches. At 0.25 A and 0.5 A, the CO_2 flow rates were 1.96 mL·min^{-1} and 3.92 mL·min^{-1}, respectively

by reducing the limitation and making almost all H_2 be utilized by the culture.

CO_2 uptake efficiency

The CO_2 uptake efficiency (Fig. 6) was consistent with electron balance. To facilitate the acclimation of the microbial community, the reactor was operated under 0.25 A in the first two days. And the CO_2 uptake efficiency of the reactor with SiO_2 NPS reached 100%. Then, the applied current and the flow rate of CO_2 were doubled. As shown in Fig. 6, the CO_2 uptake efficiency with SiO_2 NPS was over 60% except for some slight fluctuations, while the CO_2 uptake efficiency without SiO_2 NPS was between 30% and 70%. After that, the rapidly decreased CO_2 uptake efficiency might be caused by product inhibition during the last two days of each batch. All these results indicated that the addition of SiO_2 NPS could increase the CO_2 uptake efficiency of the reactor.

In a broader context, SiO_2 NPS may improve gas solubilities in water for a series of small non-polar gases, such as N_2 and CH_4, whose solubilities in an aqueous medium are also rate-limiting. We propose that SiO_2 NPS are also potentially applicable for biologically catalyzed N_2 fixation and CH_4 functionalization (Rodrigues et al. 2019), two challenging processes in small molecule activation.

Comparison to other MES reactors

The performance of this H_2-mediated MES reactor was compared to other reported MES reactors in Table 1. Most studies were devoted to improving biofilm formation by developing effective cathodes. Apparently, the current density and acetate production rate of 3D porous cathodes were much higher than those of 2D cathodes in most reported MES reactors. It was simply because the 3D porous cathode could provide a higher specific surface area for the microorganisms and formed a thicker biofilm on the electrode. To our best knowledge, the acetate production rate of all reported MES reactors was less than 1.06 g·L^{-1}·d^{-1}, and the maximum acetate concentration was around 10 g·L^{-1}. By contrast, the acetate production rate and acetate titer of this reactor containing SiO_2 NPS could reach 2.14 g·L^{-1}·d^{-1} and 18.5 g·L^{-1}, respectively, which were about twice those of the reported reactors.

These results could be partly attributed to the better mass transfer to suspended cells in the reactor. Compared to biofilm, the suspended cells had lower limitations

Table 1 Performance of most acetate-producing MES ($Q_{Surface}$: Surface production rate; $Q_{Volumetric}$: Volumetric production rate.)

Cathode material	Inoculum	$V_{catholyte}$ (L)	J ($A \cdot m^{-2}$)	$Q_{Surface}$ ($g \cdot m^{-2} \cdot d^{-1}$)	$Q_{Volumetric}$ ($g \cdot L^{-1} \cdot d^{-1}$)	Titer ($g \cdot L^{-1}$)	CE (%)	Refs
Chitosan-coated carbon cloth	*Sporomusa* ovata	0.2	0.47	13.51	0.317	0.59	86	Zhang et al. 2013
Pr0.5BSCF-CF	Mixed culture	–	− 5.6	96	0.24	7.31	73	Tian et al. 2020
CF with fluidized GAC	Mixed culture	0.28	− 4	–	0.14	3.9	65	Dong et al. 2018
Mo_2C-CF	Mixed culture	0.28	− 15	87.5	0.15	4.5	55	Huang et al. 2020
Graphite granules	Mixed culture	0.075	–	–	1.04	10.5	69	Marshall et al. 2013
rGO-CF	Mixed culture	0.28	− 4.9	68	0.17	7.1	77	Song et al. 2017
CNTs–RVC	Mixed culture	0.25	37	195	0.03	1.65	78	Jourdin et al. 2014
CF	Mixed culture	0.25	− 5	19	0.06	1.29	58	Patil et al. 2015
Carbon felt	Mixed culture	0.35	5	20.4	0.58	13.5	61	Gildemyn et al. 2015
VITO–CoRE	Mixed culture	0.5	0.069	46.7	0.14	4.97	45.5	Mohanakrishna et al. 2018
Graphene-carbon felt	*Sporomusa* ovata	0.25	− 0.23	62.4	0.124	1.88	83	Aryal et al. 2016
CNTs-coated Porous Ni hollow fiber	*Sporomusa ovata*	0.125	0.332	14.82	0.172	0.084	83	Bian et al. 2018
Carbon felt	Mixed culture	0.2	5	11.5	1.06	5.7	63	Arends et al. 2017
SS	Mixed culture	0.6	39	102	2.14	18.5	44	This work

caused by the substrate and product diffusion and electrode surface area, which could significantly improve the production rate of the bacteria. Furthermore, the addition of SiO_2 NPS further increased the mass transfer rate of dissolved H_2. However, nanoparticles could aggregate and gravitationally settle down in the stagnant flow region (dead zone) in the reactor. Moreover, the behavior of nanoparticles penetrating the cell cytoplasm may be toxic to the cell (Hwang et al. 2008). To obtain the best performance of acetate production, the optimum type and concentration of nanoparticles need to be further studied. In addition, many strategies, such as developing 3D structures and modifying functional groups on the surface of the nanoparticle could be utilized to increase the mass transfer rate and recyclability of nanoparticles. In the future, we could centrifuge the effluent to test whether it is possible to recover the silica nanoparticles for reuse, and we could also modify the silica nanoparticles into magnetic silica nanoparticles to reuse them.

Conclusion

In summary, this work developed a novel strategy, i.e., adding SiO_2 NPS, to improve the H_2 solubility in the H_2-mediated MES reactor. We found that the addition of SiO_2 NPS in the MES system could significantly increase the H_2 mass transfer rate and maximum saturated H_2 solubility in water to accelerate the production rate and titer of acetate. With the addition of 0.3wt% SiO_2 NPS, the H_2 K_{La} of the reactor increased by 32.4% at 0.5 A. The titer of acetate in batch 2 of the reactor with SiO_2 NPS ($18.5\ g \cdot L^{-1}$) was 56.9% higher than the reactor without SiO_2 NPS ($11.8\ g \cdot L^{-1}$). In the stable increment phase, the average acetate production rate of the reactor with SiO_2 NPS reached $2.14\ g \cdot L^{-1} \cdot d^{-1}$, which was much higher than other reports. This pioneering effort made with the addition of SiO_2 NPS provided insights for the development of effective microbial electrosynthesis applications. In a broader context, the nanoparticle can also be utilized in other H_2-dependent reactions, such as biologically catalyzed N_2 fixation, CH_4 functionalization and microbial protein production.

Abbreviations

MES	Microbial electrosynthesis
CEM	Cation exchange membrane
CE	Coulombic efficiency
K_{La}	Volumetric mass transfer coefficient
EET	Extracellular electron transfer
SiO_2 NPS	Silica nanoparticles
PPU	Porous polyurethane
E-CSTR	Electrochemical continuous stirred-tank reactor

Supplementary Information

The online version contains supplementary material available at https://doi.org/10.1186/s40643-023-00627-6.

Additional file 1: **Figure S1**. SEM of the SiO_2 NPS. **Figure S2**. Dissolved H_2 concentration curves (A) and K_{La} of H_2 (B) of reactors at 0.25 A. **Figure S3**. H_2 uptake efficiency (A) and CE (B) of the MES reactor in two batches. **Table S1**. Composition of trace element solution and vitamin solution.

Acknowledgements
Not applicable.

Author contributions
ZP: conceptualization, visualization, writing and editing, experiment. ZL: writing and editing and validation. XH: writing and editing and validation. KC: editing. WC: editing. KG: supervision, validation, conceptualization, writing and editing. All authors read and approved the final manuscript.

Funding
This work was sponsored by the National Natural Science Foundation of China (No. 22008194), the Natural Science of Shaanxi (No.2020JM-042, No. 2021JQ-012, and No. 2022JQ-087), China Postdoctoral Science Foundation (No.2020M673414, and No. 2020M683502).

Availability of data and materials
All data generated or analyzed during this study are included in this article.

Declarations

Ethics approval and consent to participate
Not applicable.

Consent for publication
Not applicable.

Competing interests
The authors declare that they have no competing interests.

Author details
[1]School of Chemical Engineering and Technology, Xi'an Jiaotong University, Xi'an 710049, China. [2]College of Veterinary Medicine, Northwest A&F University, Yangling 712100, China. [3]School of Ecology and Environment, Zhengzhou University, Zhengzhou 450001, China.

Received: 27 October 2022 Accepted: 9 January 2023
Published online: 20 January 2023

References

Arends JBA, Patil SA, Roume H, Rabaey K (2017) Continuous long-term electricity-driven bioproduction of carboxylates and isopropanol from CO_2 with a mixed microbial community. J CO_2 Util 20:141–149
Aryal N, Halder A, Tremblay P-L, Chi Q, Zhang T (2016) Enhanced microbial electrosynthesis with three-dimensional graphene functionalized cathodes fabricated via solvothermal synthesis. Electrochim Acta 217:117–122
Aryal N, Ammam F, Patil SA, Pant D (2017) An overview of cathode materials for microbial electrosynthesis of chemicals from carbon dioxide. Green Chem 19(24):5748–5760
Beckers L, Masset J, Hamilton C, Delvigne F, Toye D, Crine M, Thonart P, Hiligsmann S (2015) Investigation of the links between mass transfer conditions, dissolved hydrogen concentration and biohydrogen production by the pure strain *Clostridium butyricum* CWBI1009. Biochem Eng J 98:18–28
Bian B, Alqahtani MF, Katuri KP, Liu D, Bajracharya S, Lai Z, Rabaey K, Saikaly PE (2018) Porous nickel hollow fiber cathodes coated with CNTs for efficient microbial electrosynthesis of acetate from CO_2 using *Sporomusa ovata*. J Mater Chem A 6(35):17201–17211
Cai W, Cui K, Liu Z, Jin X, Chen Q, Guo K, Wang Y (2022) An electrolytic-hydrogen-fed moving bed biofilm reactor for efficient microbial electrosynthesis of methane from CO_2. Chem Eng J 132093
Cheng S, Logan BE (2007) Sustainable and efficient biohydrogen production via electrohydrogenesis. P Natl Acad Sci USA 104(47):18871–18873
Claassens NJ, Cotton CAR, Kopljar D, Bar-Even A (2019) Making quantitative sense of electromicrobial production. Nat Catal 2(5):437–447
Dong Z, Wang H, Tian S, Yang Y, Yuan H, Huang Q, Song TS, Xie J (2018) Fluidized granular activated carbon electrode for efficient microbial electrosynthesis of acetate from carbon dioxide. Bioresour Technol 269:203–209
Fruehauf HM, Enzmann F, Harnisch F, Ulber R, Holtmann D (2020) Microbial electrosynthesis-an inventory on technology readiness level and performance of different process variants. Biotechnol J 15(10):e2000066
Gildemyn S, Verbeeck K, Slabbinck R, Andersen SJ, Prévoteau A, Rabaey K (2015) Integrated production, extraction, and concentration of acetic acid from CO_2 through microbial electrosynthesis. Environ Sci Technol Lett 2(11):325–328
Huang H, Huang Q, Song TS, Xie J (2020) In situ growth of Mo_2C on cathodes for efficient microbial electrosynthesis of acetate from CO_2. Energy Fuels 34(9):11299–11306
Hwang ET, Lee JH, Chae YJ, Kim YS, Kim BC, Sang BI, Gu MB (2008) Analysis of the toxic mode of action of silver nanoparticles using stress-specific bioluminescent bacteria. Small 4(6):746–750
Jourdin L, Burdyny T (2021) Microbial electrosynthesis: where do we go from here? Trends Biotechnol 39(4):359–369
Jourdin L, Freguia S, Donose BC, Chen J, Wallace GG, Keller J, Flexer V (2014) A novel carbon nanotube modified scaffold as an efficient biocathode material for improved microbial electrosynthesis. J Mater Chem A 2(32):13093–13102
Kim YK, Park SE, Lee H, Yun JY (2014) Enhancement of bioethanol production in syngas fermentation with *Clostridium ljungdahlii* using nanoparticles. Bioresour Technol 159:446–450
Krieg T, Sydow A, Schroder U, Schrader J, Holtmann D (2014) Reactor concepts for bioelectrochemical syntheses and energy conversion. Trends Biotechnol 32(12):645–655
Liu C, Gallagher JJ, Sakimoto KK, Nichols EM, Chang CJ, Chang MC, Yang P (2015) Nanowire-bacteria hybrids for unassisted solar carbon dioxide fixation to value-added chemicals. Nano Lett 15(5):3634–3639
Liu C, Colón BC, Ziesack M, Silver PA, Nocera DG (2016) Water splitting-biosynthetic system with CO_2 reduction efficiencies exceeding photosynthesis. Science 352(6290):1210–1213
Logan BE, Rabaey K (2012) Conversion of wastes into bioelectricity and chemicals by using microbial electrochemical technologies. Science 337(6095):686–690
Marshall CW, Ross DE, Fichot EB, Norman RS, May HD (2013) Long-term operation of microbial electrosynthesis systems improves acetate production by autotrophic microbiomes. Environ Sci Technol 47(11):6023–6029
Mohanakrishna G, Vanbroekhoven K, Pant D (2018) Impact of dissolved carbon dioxide concentration on the process parameters during its conversion to acetate through microbial electrosynthesis. React Chem Eng 3(3):371–378
Myung J, Kim M, Pan M, Criddle CS, Tang SK (2016) Low energy emulsion-based fermentation enabling accelerated methane mass transfer and growth of poly(3-hydroxybutyrate)-accumulating methanotrophs. Bioresour Technol 207:302–307
Nevin KP, Hensley SA, Franks AE, Summers ZM, Ou J, Woodard TL, Snoeyenbos-West OL, Lovley DR (2011) Electrosynthesis of organic compounds from carbon dioxide is catalyzed by a diversity of acetogenic microorganisms. Appl Environ Microbiol 77(9):2882–2886
Patil SA, Arends JB, Vanwonterghem I, van Meerbergen J, Guo K, Tyson GW, Rabaey K (2015) Selective enrichment establishes a stable performing community for microbial electrosynthesis of acetate from CO_2. Environ Sci Technol 49(14):8833–8843
Prevoteau A, Carvajal-Arroyo JM, Ganigue R, Rabaey K (2020) Microbial electrosynthesis from CO_2: forever a promise? Curr Opin Biotechnol 62:48–57
Rodrigues RM, Guan X, Iñiguez JA, Estabrook DA, Chapman JO, Huang S, Sletten EM, Liu C (2019) Perfluorocarbon nanoemulsion promotes the delivery of reducing equivalents for electricity-driven microbial CO_2 reduction. Nat Catal 2(5):407–414
Salehizadeh H, Yan N, Farnood R (2020) Recent advances in microbial CO_2 fixation and conversion to value-added products. Chem Eng J 390:124584
Song TS, Zhang H, Liu H, Zhang D, Wang H, Yang Y, Yuan H, Xie J (2017) High efficiency microbial electrosynthesis of acetate from carbon dioxide by a self-assembled electroactive biofilm. Bioresour Technol 243:573–582
Tian S, He J, Huang H, Song TS, Wu X, Xie J, Zhou W (2020) Perovskite-based multifunctional cathode with simultaneous supplementation of substrates and electrons for enhanced microbial electrosynthesis of organics. ACS Appl Mater Interfaces 12(27):30449–30456
Xue X, Liu Z, Cai W, Cui K, Guo K (2022) Porous polyurethane particles enhanced the acetate production of a hydrogen-mediated microbial electrosynthesis reactor. Bioresour Technol Rep 18:101073

Zhang T, Nie H, Bain TS, Lu H, Cui M, Snoeyenbos-West OL, Franks AE, Nevin KP, Russell TP, Lovley DR (2013) Improved cathode materials for microbial electrosynthesis. Energy Environ Sci 6(1):217–224
Zhu H, Shanks BH, Heindel TJ (2008) Enhancing CO-water mass transfer by functionalized MCM41 nanoparticles. Ind Eng Chem Res 47(20):7881–7887

Publisher's Note